HHS Public Access

Author manuscript

Nat Cell Biol. Author manuscript; available in PMC 2015 August 01.

Published in final edited form as:

Nat Cell Biol. 2015 February ; 17(2): 170–182. doi:10.1038/ncb3090.

Periostin Secreted by Glioblastoma Stem Cells Recruits M2 Tumor-associated Macrophages and Promotes Malignant Growth

Wenchao Zhou[1], **Susan Q. Ke**[1], **Zhi Huang**[1], **William Flavahan**[1], **Xiaoguang Fang**[1], **Jeremy Paul**[1], **Ling Wu**[2], **Andrew E. Sloan**[3], **Roger E. McLendon**[4], **Xiaoxia Li**[2], **Jeremy N. Rich**[1], and **Shideng Bao**[1,*]

[1]Department of Stem Cell Biology and Regenerative Medicine, Lerner Research Institute, Cleveland Clinic, Cleveland, OH 44195, USA

[2]Department of Immunology, Lerner Research Institute, Cleveland Clinic, Cleveland, OH 44195, USA

[3]Departments of Neurological Surgery & Pathology, University Hospitals, Case Medical Center & Case Comprehensive Cancer Center, Case Western Reserve University School of Medicine, Cleveland, OH 44106, USA

[4]Department of Pathology, Duke University Medical Center, Durham, NC 27710, USA

Abstract

Tumor-associated macrophages (TAMs) are enriched in glioblastoma (GBM) that contains glioma stem cells (GSCs) at the apex of its cellular hierarchy. The correlation between TAM density and glioma grade suggests a supportive role of TAMs in tumor progression. Here we interrogated the molecular link between GSCs and TAM recruitment in GBMs and demonstrated that GSCs secrete Periostin (POSTN) to recruit TAMs. TAM density correlates with POSTN levels in human GBMs. Silencing POSTN in GSCs markedly reduced TAM density, inhibited tumor growth, and increased survival of mice bearing GSC-derived xenografts. We found that TAMs in GBMs are not brain-resident microglia, but mainly monocyte-derived macrophages from peripheral blood. Disrupting POSTN specifically attenuated the tumor supportive M2 type of TAMs in xenografts. POSTN recruits TAMs through integrin $\alpha_v\beta_3$ as blocking this signaling by an RGD peptide inhibited TAM recruitment. Our findings highlight the possibility of improving GBM treatment by targeting POSTN-mediated TAM recruitment.

*Correspondence should be addressed to: Shideng Bao, Department of Stem Cell Biology & Regenerative Medicine, Lerner Research Institute, Cleveland Clinic, 9500 Euclid Avenue, NE30, Cleveland, OH 44195, USA; Tel: +1 216 636 1009; Fax: +1 216 636 5454; baos@ccf.org.

AUTHOR CONTRIBUTIONS

W.Z. and S.B. designed the experiments, analyzed data and prepared the manuscript. W.Z., S.Q.K., Z.H., X.F., J.P. and L.W. performed the experiments. W.F. performed database analysis. A.E.S. and R.E.M. provided GBM surgical specimens. R.E.M. performed pathological analyses. J.N.R. and X.L. provided scientific inputs and helped to edit the manuscript.

The authors declare no competing financial interests.

Keywords

POSTN; Tumor-associated macrophage (TAM); Glioblastoma (GBM); Cancer stem cell; Microglia

Introduction

Glioblastoma multiforme (GBM) is the most common and lethal type of primary brain tumor[1]. The median survival of GBM patients is less than 16 months despite optimal treatment[2]. Abundant macrophage infiltration is a common feature of GBMs, but these tumor-associated macrophages (TAMs) in GBMs lack apparent phagocytic activity[3]. In addition, an inverse correlation between TAM infiltration and GBM prognosis has been reported[4]. Recent studies suggested that TAMs may promote GBM tumor progression in multiple aspects[5–8]. The TAM-secreted cytokines, including IL-6 and IL-10, have been shown to promote cancer cell proliferation in GBMs[8]. TAMs could also facilitate GBM tumor growth by promoting neo-vascularization[6, 7]. Moreover, TAMs can interfere with the anti-tumor functions of other immune cells[5], although TAMs do not display traditional immunocyte properties. Thus, TAMs mainly play a tumor-supportive role in GBM progression. As pioneer immunotherapies have shown initial promise for GBM treatment, interrogating immunologic regulation in GBMs may inform therapy[9–11]. In addition, since TAMs in GBM may originate from either monocytes from peripheral blood or resident microglia in brain, identifying the source of TAMs in GBMs will provide critical information to determine the appropriate therapeutic approaches. Therefore, determining the cellular and molecular mechanisms underlying TAM recruitment may facilitate the development of therapeutics to effectively improve GBM treatment.

Macrophages can be categorized into M1 and M2 subtypes based on their polarization status[12]. In tumors, the M1 or M2 subtype TAMs represent tumor suppressive or tumor supportive macrophages, respectively[13]. Cell surface markers including Iba1 and CD11b are commonly used to label total TAMs[12, 14]. Several surface markers such as CD163, Fizz1 and Arg1 have been used to mark M2 subtype TAMs, while other surface markers including MHCII, CD11c and iNOS have been suggested for M1 subtype TAMs[15–19]. Although TAMs in lower grade astrocytomas were strongly stained with the M1 marker MHCII[20], TAMs in GBM tumors manifested strong M2 marker staining[15, 21]. Such correlation between tumor grades and the M2 TAM abundance further suggests that the M2 type TAMs might play a critical role in GBM progression. However, TAMs in GBMs may be derived from circulating monocytes or resident microglia[13, 16]. Despite the fact that these two populations may share some surface markers in brain[17, 18], the studies using CX3CR1(+/GFP)-CCR2(+/RFP) knock-in fluorescent protein reporter mice demonstrated that microglia are $CX3CR1^{+}/CCR2^{-}$ but the monocyte-derived macrophages are $CCR2^{+}/CX3CR1^{-}$ [22], indicating that microglia and monocyte-derived macrophages in brains are different populations with distinct and specific surface antigens.

GBM displays remarkable cellular heterogeneity and differentiation hierarchy of cancer cells containing glioma stem cells (GSCs) that are able to self-renew, differentiate and

repopulate the whole tumor bulk[23–25]. GSCs contribute to GBM tumor growth, vascularization, and therapeutic resistance[26, 27]. GSCs are localized and maintained in the specific microenvironment called niches within a GBM tumor. Surprisingly, the GSC niches are also enriched with TAMs[28–30]. Both TAMs and GSCs are abundant in the proximity of blood vessels known as perivascular niche[28, 31, 32]. In the hypoxic regions within GBM tumors, high density of $CD11b^+$ and $F4/80^+$ TAMs can be detected[29, 30, 33]. Consistently, several lines of evidence highlighted the enhanced propagation of GSCs in the hypoxic regions[30, 33]. Furthermore, similar to the concurrence between the increased GSC population and GBM relapse[19, 34], correlation between TAM re-infiltration and tumor recurrence is often detected in GBMs[35]. These phenomena strongly suggest the interrelationship between GSCs and TAMs in GBM tumors.

To interrogate the molecular link between GSCs and TAM recruitment, we screened for candidate chemoattractants of TAMs from GSC secreted proteins. We identified Periostin (POSTN) as a potent TAM attractant that is preferentially expressed in GSCs. POSTN (originally called OSF-2) is a member of the Fasciclin family and a disulfide-linked cell adhesion protein[36]. POSTN is involved in various aspects of tumorigenic processes through signaling pathways such as Akt/PI3K, integrin and Wnt-1[37, 38]. Recently, POSTN was shown to be preferentially upregulated in stromal fibroblasts of breast cancer and help the maintenance of breast cancer stem cells by increasing Wnt signaling, thus POSTN plays a supportive role in cancer stem cell metastatic colonization and breast cancer metastasis[38]. In addition, POSTN plays crucial roles to promote tumor progression including growth, invasion and metastasis in several malignant cancers[36, 38, 39]. In this study, we found that TAM density positively correlates with POSTN protein levels in human GBMs. Disrupting POSTN dramatically reduced TAM density, inhibited tumor growth, and increased the survival of mice bearing the GSC-derived xenografts. We determined that TAMs in GBMs are mainly monocyte-derived macrophages ($CCR2^+/CX3CR1^-$) from peripheral blood but not resident microglia ($CX3CR1^+/CCR2^-$) from brain. Silencing POSTN specifically attenuated the tumor supportive M2 type ($CD163^+/Fizzl^+$) of TAMs in GSC-derived tumors. We further demonstrated that POSTN mediates through integrin $\alpha_v\beta_3$ to recruit TAMs *in vivo*. Thus, POSTN secreted by GSCs recruits M2 type of TAMs to support GBM growth.

RESULTS

POSTN is preferentially secreted by GSCs and correlates with TAM density in primary GBMs

To investigate the potential molecular link between GSCs and TAM recruitment, we screened for the GSC-secreted specific factors that can potently attract macrophages (primed U937) in the *in vitro* migration and invasion assays. First, we determined several secreted factors differentially expressed by GSCs through RT-qPCR analysis (qPCR array) and identified Periostin (POSTN) as one of the most abundantly expressed cytokines in GSCs (Supplementary Table 1). The transwell migration and invasion assays indicated that POSTN is a dominant chemoattractant to attract the primed U937 macrophage-like cells in (Supplementary Fig. 1a and 1b). Bioinformatic analyses of the TCGA database showed that POSTN expression negatively correlates with overall and progression-free survival of GBM

patients (Supplementary Fig. 1c and 1d). To interrogate the potential link between POSTN expression and GBM tumor growth, we examined the pattern of POSTN expression in human GBM surgical specimens by immunofluorescence and found that POSTN is preferentially expressed by cancer cells expressing GSC markers (SOX2 and OLIG2) and distributed in the area around GSCs (Fig. 1a, 1b and Supplementary Fig. 1e). To confirm the differential expression of POSTN in GSCs, we measured POSTN protein levels in matched GSCs and non-stem tumor cells (NSTCs) and found that GSCs preferentially expressed much higher levels of POSTN relative to NSTCs (Fig. 1c). Consistently, conditioned media from GSCs contain much more POSTN protein than that from matched NSTCs (Fig. 1d). These data demonstrate that POSTN is preferentially secreted by GSCs in human GBMs. As GSCs and TAMs are both enriched in perivascular niches in GBMs, we next examined the potential link between POSTN expression and TAM density in primary GBMs in tissue microarrays. Immunofluorescence with antibodies against POSTN and the macrophage marker Iba1 confirmed that TAMs are enriched in POSTN-abundant regions (Fig. 1e and Supplementary Fig. 1f and 1g). Immunohistochemistry confirmed that GBMs with higher levels of POSTN contain higher density of TAMs (Fig. 1f and 1g), suggesting a positive correlation between POSTN expression levels and TAM density in human GBMs.

Silencing POSTN in GSCs reduces TAM recruitment, inhibits tumor growth, and extends survival of mice bearing GSC-derived xenografts

To address whether GSC-secreted POSTN plays a role in TAM recruitment and GBM tumor growth, we examined the effect of POSTN knockdown on TAM density and tumor growth in GSC-derived GBM xenografts. Lentiviral mediated shRNA silencing reduced POSTN expression in GSCs by 85–90% (Fig. 2a and Supplementary Fig. 2a). GSCs expressing POSTN shRNAs (shPOSTN) or non-targeting shRNA (shNT) and firefly luciferase were transplanted into immunocompromised mice through intracranial injection. Bioluminescent imaging of orthotopic tumors *in vivo* showed a dramatic inhibition of tumor growth in the xenografts derived from GSCs expressing shPOSTN relative to those expressing shNT (Fig. 2b). Consistently, silencing POSTN also significantly extended the survival of mice bearing the GSC-derived tumors (Fig. 2c and Supplementary Fig. 2b and 2c). These data demonstrate a supportive role of POSTN in GBM tumor growth. Given that POSTN protein levels showed a positive correlation with TAM density in primary GBMs, we next examined the impact of POSTN down-regulation on TAM density in the GSC-derived xenografts with immunofluorescence staining of two well-defined macrophage makers Iba1 and CD11b[40, 41]. TAM density was dramatically reduced by more than 65% in the tumors derived from GSCs expressing shPOSTN while abundant TAMs were present in control tumors derived from shNT-transduced GSCs (Fig. 2d–2f, Supplementary Fig. 2d–2e and 3a–3c). We confirmed that Iba1 and CD11b staining overlapped in marking TAMs in GBM intracranial xenografts (Supplementary Fig. 3d) and the isolated TAMs from the subcutaneous xenografts (Supplementary Fig. 3e). Collectively, these data demonstrate that GSC-secreted POSTN plays critical roles in promoting TAM recruitment and GBM tumor growth.

TAMs in GBM are monocyte-derived macrophages from peripheral blood

As the origin of TAMs in GBM has not been well defined, we next sought to address whether TAMs recruited by POSTN in GBM tumors are monocyte-derived macrophages from peripheral blood or resident microglia from brain. Previous reports have shown that microglia within normal brain are $CX3CR1^{+}/CCR2^{-}$ while the monocyte-derived macrophages are $CCR2^{+}/CX3CR1^{-}$ [22, 42], so we applied these markers to analyze the TAMs in GSC-derived xenografts and primary GBM tumors. Consistently, the majority of macrophages were $CX3CR1^{+}/CCR2^{-}$ within the normal mouse brain (Fig 3a, bottom panels), confirming they were resident microglia. However, only $CCR2^{+}/CX3CR1^{-}$ macrophages were found in the GSC-derived GBM xenografts (Fig 3a, top panels), demonstrating that POSTN-recruited TAMs in GBMs were monocyte-derived macrophages from peripheral blood. We further validated that TAMs in the majority of human primary GBMs were also $CCR2^{+}/CX3CR1^{-}$, the monocyte-derived macrophages (Fig. 3b–3c and Supplementary Fig. 4a). Moreover, we found that TAMs were enriched around blood vessels in primary GBMs and the GSC-derived xenografts (Fig. 3d and 3e). These data demonstrate that the recruited TAMs in GBMs are mainly monocyte-derived macrophages originated from peripheral blood.

Disrupting POSTN in GSCs specifically reduces M2 tumor supportive TAMs *in vivo*

Recent studies indicated that there are at least two subtypes (M1 and M2) of TAMs in tumors[43–45]. The M1 subtype has an inhibitory effect on tumor growth whereas the M2 subtype plays a supportive role to promote tumor progression by secreting cell growth cytokines and survival factors[46–48]. To address which subtype of TAMs was recruited or maintained by POSTN in GBM tumors, we applied M2-specific markers (Fizz-1, CD163, and Arg1)[15, 49, 50] and M1-specific markers (MHCII and CD11c)[14, 51] to distinguish TAMs in GSC-derived tumors. More than 50% of TAMs in control tumors derived from GSCs expressing shNT were M2 subtype TAMs as they were positive for Fizz-1, CD163 and Arg1 (Fig. 4a–4i), which mimics the situation in primary GBMs (Supplementary Fig. 4b–4g). However, the M2 TAMs ($Fizz\text{-}1^{+}$, $CD163^{+}$ or $Arg1^{+}$) were markedly reduced in the GBM tumors derived from GSCs expressing shPOSTN (Fig. 4a–4i), indicating that disrupting POSTN in GSCs attenuated the M2 TAMs in the GSC-derived tumors. Consistently, overexpression of POSTN in GSCs accelerated xenograft growth and increased M2 TAM recruitment (Fig. 4j and 4k). In addition, a fraction (<50%) of TAMs was positive for the M1 subtype markers MHCII and CD11c in tumors derived from shNT-transduced GSCs (Fig. 5a–5f). In contrast, the majority of TAMs in the GBM tumors derived from GSCs expressing shPOSTN showed positive staining for the M1 markers MHCII and CD11c (Fig. 5a–5f), although total TAMs were dramatically reduced in the POSTN-silencing tumors relative to POSTN-expressing tumors. In addition, F4/80, a marker for macrophage maturation[52], was detected in most TAMs (76%~88%) within POSTN-silencing tumors (Fig. 5g–5i). However, only a small proportion (10–15%) of TAMs in the tumors derived from shNT-transduced GSCs were F4/80 positive (Fig. 5g–5i), suggesting an inhibition of macrophage maturation by POSTN in GBM tumors. Collectively, these data indicate that GSC-secreted POSTN also plays a critical role in maintaining the M2 subtype of TAMs in GBM tumors.

To further validate the role of POSTN in regulating M1/M2 subtype of TAMs, we applied qPCR to determine the expression of multiple M2 and M1 markers in TAMs. $CD11b^+$ cells in GBM xenografts were isolated by magnetic assisted cell sorting (MACS). When we examined M1/M2 marker expression in the $CD11b^+$ populations from xenografts derived from shNT- or shPOSTN-expressing GSCs, we detected a significant down-regulation of the M2 markers STAB1 and Lyve1 but a substantial up-regulation of the M1-specific markers CCL17 and IL1b[43] in the $CD11b^+$ TAMs isolated from the xenografts derived from POSTN-silencing GSCs (Fig. 5j). These data further confirmed that POSTN not only recruits TAMs but also maintains the M2 subtype of TAMs in GBMs.

POSTN displays potent capacity to recruit macrophages/monocytes

To validate whether POSTN functions as a potent GSC-secreted chemoattractant, we performed a series of migration and invasion assays to examine the capacity of POSTN to attract macrophages/monocytes. Conditioned media from GSCs attracted significantly more PMA-primed macrophage-like U937 cells than the media from matched non-stem tumor cells (Fig. 6a and 6b). Pre-incubation of GSC conditioned media with an anti-POSTN antibody attenuated the promoting effect of macrophage migration (Fig. 6c and 6d). Furthermore, silencing POSTN expression in GSCs by two specific shRNAs also significantly reduced such chemoattractant effect (Fig. 6e and 6f). When exogenous POSTN was overexpressed in non-stem tumor cells (Fig. 6g), the resultant conditioned media displayed dramatically increased ability to attract the U937-derived macrophage-like cells (Fig. 6h–6i). The capacity of POSTN to attract monocyte/macrophages was further demonstrated with the isolated human primary monocytes in migration and invasion assays (Fig. 6j–6m). To further address whether POSTN-mediated attractant effect is dose-dependent, we examined the impact of different concentrations of recombinant POSTN (rPOSTN) protein on macrophage migration. The migration of U937 macrophages toward POSTN was significantly enhanced with increase of rPOSTN protein (Fig. 6n and 6o), indicating that POSTN attracts macrophages in a dose-dependent manner. Collectively, these data demonstrate that POSTN preferentially secreted by GSCs displays potent capacity to attract macrophages.

POSTN recruits TAMs via integrin $\alpha_v\beta_3$ signaling

Next, we turned attention to the molecular mechanisms underlying the POSTN-mediated recruitment of TAMs. Previous reports suggested that integrin $\alpha_v\beta_3$ is the key receptor for POSTN in mediating cell migration[53, 54]. Immunofluorescence staining showed that TAMs in GBM xenografts and primary GBM tumors express integrin $\alpha_v\beta_3$ (Fig. 7a and 7b), suggesting that the POSTN-integrin $\alpha_v\beta_3$ axis may regulate TAMs recruitment. To elucidate the signaling mediated by POSTN for TAM recruitment, we examined whether GSC-secreted POSTN can activate integrin $\alpha_v\beta_3$ on monocyte-derived macrophages *in vitro*. We applied the U937 line that can be primed from monocytes to macrophage-like cells[55, 56] for the study, as most of the PMA-primed U937 cells are integrin $\alpha_v\beta_3$ positive (Fig. 7c). Consistently, POSTN induced activation of Akt in the primed U937 cells, which can be blocked by addition of anti-integrin $\alpha_v\beta_3$ antibody (Fig. 7d), indicating that POSTN can activate integrin $\alpha_v\beta_3$ pathway in macrophages. We then examined the impact of an integrin inhibitory RGD peptide (Arg-Gly-Asp-d-Phe-Lys) related to a clinically developed anti-

tumor agent, Cilengitide[57], on POSTN-mediated recruitment of U937 macrophages. Disruption of the integrin signaling in U937 cells by the RGD inhibitory peptide significantly attenuated the recruitment of the macrophages by rPOSTN protein (Fig. 7e and 7f), suggesting that integrin $\alpha_v\beta_3$ on macrophage surface is involved in the response to POSTN. To confirm whether the POSTN-integrin $\alpha_v\beta_3$ axis plays a critical role in the POSTN-mediated TAM recruitment *in vivo*, we further investigated the inhibitory effect on TAMs recruitment by the RGD peptide in GSC-derived GBM xenografts. Surprisingly, the GSC-derived tumors in the group of mice treated with the RGD peptide for 5 days showed ~70% reduction in TAM density relative to the control tumors from mice treated with a control peptide (Fig. 7g and 7h). Taken together, these data indicate that POSTN recruits TAMs through integrin $\alpha_v\beta_3$ signaling in GBM tumors.

Intracranial co-transplantation of M2 subtype TAMs with GSCs accelerates tumor growth of GSC-derived xenografts

As silencing POSTN specifically reduces M2 type of TAMs and potently inhibited tumor growth in GSC-derived xenografts, we next investigated the role of M2 TAMs in GBM tumor growth. Statistical analysis of TCGA database showed that the M2 macrophage marker CD163 negatively correlated to GBM patient survival (Supplementary Fig. 4h), but the M1 macrophage marker MHCII positively correlated to prognosis (Supplementary Fig. 4i). In addition, immunofluorescent and immunohistochemical analyses demonstrated a positive correlation between POSTN expression and M2 subtype macrophage density in human GBM specimens (Supplementary Fig. 5a–5c). POSTN treatment enhanced expression of M2 markers but reduced expression of M1 markers in mouse intraperitoneal macrophages and U937-derived macrophage-like cells (Supplementary Fig. 5d–5e), although disrupting POSTN by shRNAs showed mild impact on GSC proliferation *in vitro* (Supplementary Fig. 6a–6c). These data suggest that the M2 subtype TAMs recruited and maintained by GSC-secreted POSTN may play a critical role in GSC-derived xenograft growth. To further explore the impact of M2 subtype TAMs on GBM tumor growth, we isolated $CD11b^+$ TAMs that are enriched with M2 subtype TAMs from GSC-derived orthotopic xenografts, and then transplanted these TAMs with luciferase-expressing GSCs into mouse brains. Bioluminescent imaging demonstrated that intracranial co-transplantation of M2 TAMs with GSCs dramatically accelerated GSC tumor growth relative to the transplantation of GSCs alone (Fig. 8a). Moreover, co-transplantation of M2 TAMs with GSCs also significantly shortened the survival of animals relative to the GSC transplantation alone (Fig. 8b). In addition, co-transplantation of M2 TAMs with GSCs expressing shPOSTN partially rescued the inhibition of GSC tumor growth caused by POSTN disruption (Fig. 8c), indicating an essential role of TAMs in mediating the POSTN-promoted tumor growth. The failure to fully rescue the inhibiting effect of POSTN silencing in GSC tumor growth by the co-transplanted M2 TAMs may be ascribed to the loss of M2 properties, impacted viability, or migration away of these TAMs from the tumor due to the absence of POSTN. Collectively, these data demonstrate that the M2 subtype TAMs have potent capacity to promote GBM growth *in vivo*.

DISCUSSION

GBM often contains a large number of TAMs that constitute the dominant immune cell population within the tumor. Accumulating evidence suggests that TAMs rarely phagocytize cancer cells or behave like antigen-presenting cells[43, 58]. The M2 subtype TAMs are now widely regarded as immunosuppressive cells with a tumor supportive role[15, 43], although a role of M1 TAMs in anti-tumor immune responses has been reported[59]. Tumors may recruit TAMs via secretion of CC chemokine ligand 2 (CCL2) and soluble colony-stimulating factor 1 (sCSF1) in other cancers[60–63]. In this study, we demonstrated that TAMs in GBMs are mainly recruited by POSTN, a chemokine preferentially expressed by GSCs but rarely expressed by non-stem tumor cells or differentiated glioma cells in GBMs (Fig. 1c, 1d and Supplementary Fig. 6d–6i). GSC-secreted POSTN functions as a potent chemoattractant to recruit monocyte-derived macrophages from peripheral blood and maintain M2 subtype of TAMs to promote tumor growth in GBMs (Fig. 8d). The fact that only $CCR2^+$ macrophages but not $CX3CR1^+$ macrophages appeared in the GSC-derived GBM tumors indicates a preferential recruitment of peripheral macrophages by GSC-secreted POSTN, as CCR2 is a specific marker for monocyte-derived macrophages, whereas CX3CR1 is an indicator of resident microglia from brain[22, 42]. Consistently, we detected enrichment of TAMs around vessels (Fig. 3d and 3e). As GSCs tend to cluster in perivascular niches[28, 31, 32], GSCs may modulate their microenvironment through POSTN-mediated TAM recruitment to form a favorable niche for the survival of both GSCs and TAMs. The interplay between GSCs and TAMs may be critical to promote GBM tumor growth.

Our results demonstrated that disrupting POSTN *in vivo* significantly reduced recruitment of the tumor supportive TAMs (M2 type) and inhibited GBM tumor growth. To determine other biological effects of POSTN down-regulation in GBM tumors, we also examined the impact of targeting POSTN on several aspects of tumor biology such as vessel density, GSC population, cell proliferation and survival. POSTN knockdown had no obvious effects on vascular density in GSC-derived xenografts (Supplementary Fig. 7a–7c). Similarly, blocking POSTN-integrin $\alpha_v\beta_3$ signaling by RGD treatment didn't show significant impact on vessel density (Supplementary Fig. 7d and 7e). However, the vessel morphology changed to some degree, which may be associated with the reduced TAM density. In addition, POSTN knockdown had no significant impact on GSC populations in tumor bulk as demonstrated by SOX2 immunofluorescence (Supplementary Fig. 8a and 8b). Furthermore, there was no significant difference in cancer cell proliferation between the GSC-derived tumors expressing shPOSTN and shNT as indicated by Ki-67 staining (Supplementary Fig. 8c and 8d). In contrast, targeting POSTN induced massive apoptosis in GSC-derived xenografts as demonstrated by TUNEL assay (Supplementary Fig. 8e and 8f). Moreover, qPCR analysis demonstrated a dramatic up-regulation of M2 markers STAB1 and Lyve1 in $CD11b^+$ cells (TAMs) from GBM xenografts relative to resident microglias from normal mouse brains (Supplementary Fig. 8g). These data suggest that the reduced M2 TAMs caused by POSTN disruption might be closely associated with the increased apoptosis and inhibited tumor growth in the GBM xenografts expressing shPOSTN. Thus, POSTN-mediated recruitment and maintenance of M2 TAMs largely contributes to the accelerated tumor growth by promoting cancer cell survival in GBMs, although POSTN itself may also partially play a

direct role on promoting tumor cell survival *in vivo*. It will be important to determine how POSTN-recruited M2 TAMs augment cancer cell survival in GBMs in the future study.

Our studies uncovered the cellular and molecular mechanisms underlying the TAM recruitment in GBMs. We also identified the origin of TAMs and their subtype in this lethal type of brain tumor. GSCs preferentially secrete POSTN to recruit TAMs into GBM tumors, although other factors may also affect immune cells in GBMs. As POSTN-recruited TAMs are mainly monocyte-derived macrophages from blood, the contribution of microglia from brain to TAMs in GBMs is not as critical as we previously thought. Thus, targeting monocyte-derived TAMs should be considered as the major focus of GBM immunotherapy. Furthermore, we demonstrated that POSTN-recruited TAMs are maintained as pro-tumorigenic M2 subtype of macrophages, indicating that the recruited TAMs may produce important factors to augment GBM tumor growth. Consistently, silencing POSTN expression markedly reduced TAMs and inhibited GBM tumor growth by reducing cell survival. As previous studies in other tumors such as colon cancers have shown that POSTN promotes cancer cell survival through AKT activation[36, 37], it's likely that POSTN may affect GBM tumor growth via multiple mechanisms besides recruitment and maintenance of M2 TAMs. Thus, targeting POSTN signaling, blocking POSTN-mediated TAM recruitment and eliminating the POSTN producer GSCs are likely to be attractive therapeutic approaches. As a reciprocal supportive interplay between cancer cells and TAMs may be critical to promote tumor progression, disrupting the interrelationship between TAMs and cancer cells especially GSCs may effectively inhibit GBM tumor growth. Recently, targeting TAMs by trabectedin has been shown to exhibit a significant anti-tumor activity in lung carcinoma, ovarian cancer and fibrosarcoma[64]. Our finding of molecular mechanisms underlying the TAM recruitment by GSC-secreted POSTN may shed light on the development of therapeutics to improve GBM treatment. In addition, therapeutic targeting of POSTN-mediated TAM recruitment may synergize with current immunotherapies to effectively increase survival of patients with GBMs and possible other lethal cancers.

METHODS

Human GBM specimens and glioma-derived cells

De-identified GBM surgical specimens were collected from Cleveland Clinic Brain Tumor and Neuro-Oncology Center and the University Hospitals-Case Medical Center in accordance with Institutional Review Board-approved protocols. Informed consent was obtained from all patients. Tissue microarray slides containing 96 GBM samples were purchased from US Biomax. Characteristics of the original cancers were described previously[65]. GSCs and matched non-stem tumor (NSTCs) cells were isolated from GBM specimens or xenografts through cell sorting and functionally characterized as previously described[26, 65, 67, 68] with minor modification. Briefly, GBM tumors were disaggregated using the Papain Dissociation System (Worthington Biochemical) according to the manufacturer's instructions. Isolated cells were recovered in stem cell medium (Neurobasal-A medium with B27 supplement, 10 ng/ml EGF and 10 ng/ml bFGF) for at least 6 hours to allow re-expression of surface markers, and then sorted by fluorescence-activated cell sorting (FACS) using at least two surface markers (CD15/CD133). Cells were labeled with a

phycoerythrin (PE)-conjugated anti-CD133 antibody (Miltenyi Biotec, 130-098-826, 1:11) and the FITC-conjugated anti-CD15 antibody (Millipore, CBL144F, 1:20), and the $CD133^+$/$CD15^+$ cells were isolated through cell sorting. The enriched GSCs ($CD133^+$/$CD15^+$) were maintained in the stem cell medium and the identity was confirmed by SOX2 and OLIG2 expression and the activation of SOX2 promoter-driven GFP expression. The cancer stem cell phenotype of GSCs was validated by functional assays of self-renewal (serial neurosphere formation at the clonal density), *in vitro* induction of differentiation and tumor propagation (*in vivo* limiting dilution assay) as previously described[26,65,67,68]. After validation of the cancer stem cell phenotype by these functional assays, the sorted GSCs were used for the *in vitro* and *in vivo* experiments. The sorted CD133-/CD15− cells from matched GBM tumors were used as non-stem tumor cells (NSTCs).

Intracranial tumor formation *in vivo*

Intracranial transplantation of GSCs to establish GBM xenografts was performed as described[26, 65]. Female C57BL/6 athymic nude mice of 4–6 weeks were purchased from Charles River Laboratories. GSCs were transplanted into the right cerebral cortex at a depth of 3.5 mm through intracranial injection. Mice were euthanized when exhibiting neurological sign including domehead, haemiparesis, or more than 20% of body weight loss. All animal protocols were approved by the Animal Research Committee of the Cleveland Clinic, and all animals were housed in the Association for the Assessment and Accreditation of Laboratory Animal Care-accredited animal facility at Cleveland Clinic Lerner Research Institute. No specific method was used to predetermine sample size. The experiments were not randomized. Only animals with accidental death (for example, due to infection or intracranial injection) were excluded from the data analysis. The investigators were not blinded to allocation during experiments and outcome assessment. GSCs were transduced with expression of NT shRNA (shNT) or POSTN shRNAs (shPOSTN) along with luciferase through lentiviral infection. 48 hours after infection, 20,000 viable cells were engrafted intracranially into immunocompromised mice. Animals were monitored by bioluminescent imaging or maintained until manifestation of neurological signs.

Immunoblotting and immunofluorescent staining

Immunoblotting and immunofluorescent staining were performed as described[65, 66]. Specific antibodies against POSTN (Abcam, ab14041, 1: 400), GSC marker SOX2 (Millipore, AB5603, 1:200; Santa Cruz, sc-17320, 1:200) or OLIG2 (R&D systems, AF2418, 1:100), endothelial cell marker Glut1 (Millipore, 07-1401, 1:500) or CD31 (Dako, M082301, 1:100), and macrophage markers Iba1 (Abcam, ab5076, 1:200), CD11b (Abd serotec, MCA711GT, 1:100), Fizz1 (Abcam, ab39626, 1:100), CD163 (Santa Cruz, sc-33560, 1:100), F4/80 (Abd serotec, MCA497RT, 1:100), CX3CR1 (Abcam, ab8021, 1:100) or CCR2 (Abcam, ab32144, 1:100) were used for immunofluorescent staining on GBM tumor sections as indicated. Specific antibodies against POSTN (Abcam, ab14041, 1: 10,000), tubulin (Sigma, T8203, 1:10,000), phosphor-S473 Akt (Cell Signaling Technology, 9271, 1:1,000), Akt (Cell Signaling Technology, 9272, 1:1,000) were used for immunoblot analyses. To determine TAM density, cryosections of GBM tumors were co-stained with Iba1 (or CD11b) and Glut1. The numbers of $Iba1^+$ (or $CD11b^+$) cells were calculated by ImageJ. Glut1 positive areas were regarded as vessels and determined by ImageJ. For TAMs

density in each sample, the number of Iba1$^+$ (or CD11$^+$) cells was divided by vessel area for normalization to exclude the individual variation in vascularization. The final outcome was defined as the TAM density.

Immunohistochemical (IHC) staining

IHC staining was carried out with the ABC kit and DAB kit (Vector Laboratories) according to manufacturer's instructions. Primary antibodies for POSTN (ab14041, 1:400), Iba1 (ab5076, 1:400), CX3CR1 (ab8021, 1:100), CCR2 (ab32144, 1:100) and Ki67 (ab15580, 1:400) from Abcam were used for the IHC staining. To study the correlation between POSTN level and TAM recruitment, the sequential sections of primary GBM microarrays were stained with antibodies against POSTN or Iba1, respectively. The IHC staining of POSTN was evaluated by two independent pathologists. The samples with a score of 0~1 were regarded as low expression and those with a score of 2~4 were regarded as high expression. For Iba1 evaluation, 3 random areas from a single section were checked for Iba1$^+$ cells. If the average number of Iba1$^+$ cells was less than 100 Iba1$^+$ cells in 4.2mm^2 (2.36×1.78 mm^2), the sample was ascribed to Iba1 low. Otherwise the sample was classified as Iba1 high.

TUNEL assays

TUNEL assays detecting apoptosis in tumor sections were performed with an ApopTag Plus Peroxidase in situ apoptosis kit (Chemicon) according to manufacturer's instructions.

U937 monocyte transwell assays

U937 cells (ATCC) were cultured in the suggested medium 24 hours before priming. U937 monocytes were primed with 5nM PMA (Sigma) for 48 hours to become monocyte-derived macrophages as described[55]. Transwell assays assessing cell migration or invasion potential were performed on 24-well plate with inserts (BD Biosciences) according to manufacturer's instruction. Briefly, 5×10^5 of primed U937 cells were cultured in the upper chamber and allowed to migrate or invade for 24–48 hours before fixation for crystal purple staining. Recombinant human POSTN protein was purchased from R&D Systems. Conditioned media (CM) were obtained by culturing T387 GSCs or NSTCs in RPMI/1640 media with 0.1% BSA for 24 hours and then used for the cell migration transwell assay.

Isolation of human monocytes from blood

Human monocytes were isolated by Ficoll-plaque plus (GE healthcare) centrifugation of human blood followed by the collection of monocytes attached to the plastic surface after 4 hours culture. Briefly, blood from donors were diluted in Hank's buffer to a 1:1 solution. The blood solution was placed over half volume of Ficoll-plaque plus (GE healthcare) and centrifuged at 1,600rpm for 30 minutes. The middle layer of PBMCs were collected and cultured in RPMI/1640 medium supplemented with 10% FBS. 4 hours after culture, the floating cells were washed away with PBS. The adherent monocytes were trypsinized and subjected to migration or invasion assays. All studies related to human subjects were approved by the Institutional Review Board of the Cleveland Clinic. Informed consent was obtained from all subjects. For transwell assays, 5×10^4 human monocytes/macrophages

were cultured in the upper chamber while recombinant POSTN protein (0.5 μg/ml) in RPMI/1640 media with 0.1% BSA was added in the lower chamber. Cells were allowed to migrate or invade for 24h and the migrated cells in the bottom of the well were fixed and stained.

Isolation of CD11b$^+$ cells from GBM xenografts

Mouse brain tissues or GBM xenografts were digested with the Neural Tissue Dissociation Kit (Miltenyi Biotec) followed by MACS sorting with PE conjugated anti-CD11b antibody (Miltenyi Biotec, 130-091-240, 1:11) and anti-PE conjugated microbeads (Miltenyi Biotec). Briefly, mouse brains or tumors were washed with PBS, minced, and incubated with enzyme mixes. The dissociated brain tissue was passed through a 40μm cell strainer. Tissue was then re-suspended in a 30% Percoll (Santa Cruz) PBS solution and centrifuged at 700g for 10 minutes to remove myelin. Cells were re-suspended in 90μl IMAG buffer (PBS w/o Ca2+/Mg2+, supplemented with 0.5% BSA and 2mM EDTA, pH 7.2) plus 10μl anti-CD11b-PE (Miltenyi) and incubated on ice for 30 minutes. Cells were then washed three times with 1ml IMAG buffer and incubated with 20μl anti-PE microbeads (Miltenyi) plus 80μl IMAG buffer on ice for 15 minutes. After labeling, cells were washed, re-suspended in 500μl IMAG buffer, and applied to MS column (Miltenyi). After wash for 3 times, CD11b$^+$ cells were flushed out of the column by plunger. CD11b$^+$ cells were then cultured in RPMI/1640 medium supplemented with 10% FBS for 1 hour and used for co-injection or lysed for RNA extraction.

RGD peptide treatment *in vivo*

After manifestation of clear luciferase signals in IVIS imaging, mouse bearing GSC-derived xenografts were treated with RGD peptide (Peptides International, PCI-3661-PI) or control peptide (Peptides International, PCI-3883-PI) through intraperitoneal delivery. The peptides were dissolved in PBS at 5mg/ml and mice were continuously treated with control or RGD peptide at 25mg/kg for 5 days. 2 hours after the last injection, mice were sacrificed and brains were fixed in 4% PFA for analysis.

Isolation of mouse peritoneal macrophages

BALB/c mice of 6–8 weeks were stimulated by i.v. injection of 1 mL 3% Brewer thioglycollate medium into the peritoneal cavity. Inflammatory response was allowed for 4 days. Mice were then sacrificed and the peritoneal macrophages were harvested by washing the cavity with 1ml ice cold PBS.

shRNAs for knockdown

Lentiviral mediated shRNAs targeting POSTN (TRCN0000123055 for O55; TRCN0000123056 for O56, and TRCN0000123057 for O57) or control shRNA (SHC002) were purchased from Sigma-Aldrich.

RT-qPCR array of secreted proteins

To identify potential chemoattractants differentially expressed by GSCs, we used qPCR array (RT-qPCR analysis) to determine the expression of major secreted proteins, including most cytokines along with some secreted proteins relevant to tumorigenesis, in paired GSCs

and NSTCs. qPCR primers were designed to span an intron of each target gene (Supplementary Table 1). Total mRNA was purified from paired GSCs and NSTCs with the RNeasy Mini Kit (74104, Qiagen). 500 ng mRNA was reverse transcribed into cDNA with SuperScript III Reverse Transcriptase (18080-044, Invitrogen). RT-qPCR assays were performed with SYBR Green PCR Master Mix (4310251, Applied Biosystems) on a 7900HT thermal cycler (Applied Biosystems). Three-step amplification was performed (95°C 15 sec, 60°C 15 sec, and 72°C 30 sec) for 45 cycles. For data analysis, GAPDH was used as the internal standard and fold changes of gene expression levels in GSCs relative to NSTCs were calculated. The target genes with a > 2 fold upregulation in GSCs were regarded as differentially expressed. RT-qPCR arrays were performed with 3 pairs of matched GSCs and NSTCs and repeated for three times. Average fold changes of target genes presented were from 3 representative experiments.

Primers for other qPCR analyses

mSTAB1-qF: ACGGGAAACTGCTTGATGTC

mSTAB1-qR: ACTCAGCGTCATGTTGTCCA

mLyve1-qF: CTGGCTGTTTGCTACGTGAA

mLyve1-qR: CATGAAACTTGCCTCGTGTG

mCcl17-qF: AGTGCTGCCTGGATTACTTCAAAG

mCcl17-qR: CTGGACAGTCAGAAACACGATGG

mIL12a-qF: GGAAGCACGGCAGCAGAATA

mIL12a-qR: AACTTGAGGGAGAAGTAGGAATGG

mIL1b-qF: GTGTGGATCCAAAGCAATAC

mIL1bqR: GTCTGCTCATTCATGACAAG

mGAPDH-qF: TGATGACATCAAGAAGGTGGTGAAG

mGAPDH-qR: TCCTTGGAGGCCATGTAGGCCAT

Statistical analysis

The level of significance was determined by a two-tailed un-paired Student’s t-test (bar graphs) or analysis of variance with $\alpha = 0.05$ (survival curves) and analyzed with GraphPad Prism 5 software. All quantitative data presented are the mean ± s.e.m. from at least three samples or experiments per data point.

Repeatability of experiments

Representative transwell images and the corresponding statistical analyses (Figs. 6b–d, 6f, 6i, 6l, 6m, 6o, 7f; Supplementary Figs. 1a–b) are shown from three experiments. Immunofluorescent analyses (Figs. 2e–f, 4b–c, 4e–f, 4h–i, 4k, 5b–c, 5e–f, 5h–i, 7h; Supplementary Figs. 2e, 3b–c, 7b, 7c, 7e, 8b, 8d, 8f) are shown from three independent experiment using cryosections from 5 different xenografts. qPCR analyses (Figs. 5j; Supplementary Figs. 5d, 5e, 8g) are shown from three independent experiments.

Immunofluorescent analyses of human primary GBMs (Figs. 1b; Supplementary Figs. 4e–g) are shown from 5 patients. Immunofluorescent analyses of human primary GBMs (Supplementary Figs. 6e, 6g, 6i) are shown from 3 patients.

Supplementary Material

Refer to Web version on PubMed Central for supplementary material.

Acknowledgments

We thank the Brain Tumor and Neuro-Oncology Centers at Cleveland Clinic and University Hospitals-Case Medical Center for providing GBM surgical specimens for this study. We are grateful to members in Dr. Rich's laboratory for their assistance and scientific discussion. We also thank Cathy Shemo and Sage O'Bryant of the Flow Cytometry Core, Judith Drazba and Linda Vargo of the Imaging Core at Cleveland Clinic Lerner Research Institute, Dave Schumick of the Center for Medical Art and Photography for their assistance. This work was supported by the Cleveland Clinic Foundation and a NIH R01 grant (NS070315) to S. Bao.

References

1. Deorah S, Lynch CF, Sibenaller ZA, Ryken TC. Trends in brain cancer incidence and survival in the United States: Surveillance, Epidemiology, and End Results Program, 1973 to 2001. Neurosurg Focus. 2006; 20:E1. [PubMed: 16709014]
2. DeAngelis LM. Brain tumors. N Engl J Med. 2001; 344:114–123. [PubMed: 11150363]
3. Hao C, et al. Cytokine and cytokine receptor mRNA expression in human glioblastomas: evidence of Th1, Th2 and Th3 cytokine dysregulation. Acta Neuropathol. 2002; 103:171–178. [PubMed: 11810184]
4. Abou-Ghazal M, et al. The incidence, correlation with tumor-infiltrating inflammation, and prognosis of phosphorylated STAT3 expression in human gliomas. Clin Cancer Res. 2008; 14:8228–8235. [PubMed: 19088040]
5. Morford LA, Dix AR, Brooks WH, Roszman TL. Apoptotic elimination of peripheral T lymphocytes in patients with primary intracranial tumors. J Neurosurg. 1999; 91:935–946. [PubMed: 10584838]
6. Hirano H, Tanioka K, Yokoyama S, Akiyama S, Kuratsu J. Angiogenic effect of thymidine phosphorylase on macrophages in glioblastoma multiforme. J Neurosurg. 2001; 95:89–95. [PubMed: 11455962]
7. Kanamori M, Kawaguchi T, Berger MS, Pieper RO. Intracranial microenvironment reveals independent opposing functions of host alphaVbeta3 expression on glioma growth and angiogenesis. J Biol Chem. 2006; 281:37256–37264. [PubMed: 17028191]
8. Samaras V, et al. Application of the ELISPOT method for comparative analysis of interleukin (IL)-6 and IL-10 secretion in peripheral blood of patients with astroglial tumors. Mol Cell Biochem. 2007; 304:343–351. [PubMed: 17551671]
9. Mineharu Y, et al. Engineering the brain tumor microenvironment enhances the efficacy of dendritic cell vaccination: implications for clinical trial design. Clin Cancer Res. 2011; 17:4705–4718. [PubMed: 21632862]
10. Pellegatta S, et al. Neurospheres enriched in cancer stem-like cells are highly effective in eliciting a dendritic cell-mediated immune response against malignant gliomas. Cancer Res. 2006; 66:10247–10252. [PubMed: 17079441]
11. Graf MR, Prins RM, Hawkins WT, Merchant RE. Irradiated tumor cell vaccine for treatment of an established glioma. I. Successful treatment with combined radiotherapy and cellular vaccination. Cancer Immunol Immunother. 2002; 51:179–189. [PubMed: 12012105]
12. Sielska M, et al. Distinct roles of CSF family cytokines in macrophage infiltration and activation in glioma progression and injury response. J Pathol. 2013; 230:310–321. [PubMed: 23520016]
13. Staudt ND, et al. Myeloid cell receptor LRP1/CD91 regulates monocyte recruitment and angiogenesis in tumors. Cancer Res. 2013; 73:3902–3912. [PubMed: 23633492]

14. Pucci F, et al. A distinguishing gene signature shared by tumor-infiltrating Tie2-expressing monocytes, blood “resident” monocytes, and embryonic macrophages suggests common functions and developmental relationships. Blood. 2009; 114:901–914. [PubMed: 19383967]
15. Komohara Y, Ohnishi K, Kuratsu J, Takeya M. Possible involvement of the M2 anti-inflammatory macrophage phenotype in growth of human gliomas. J Pathol. 2008; 216:15–24. [PubMed: 18553315]
16. Ling EA, Wong WC. The origin and nature of ramified and amoeboid microglia: a historical review and current concepts. Glia. 1993; 7:9–18. [PubMed: 8423067]
17. Deininger MH, Seid K, Engel S, Meyermann R, Schluesener HJ. Allograft inflammatory factor-1 defines a distinct subset of infiltrating macrophages/microglial cells in rat and human gliomas. Acta Neuropathol. 2000; 100:673–680. [PubMed: 11078219]
18. Akiyama H, McGeer PL. Brain microglia constitutively express beta-2 integrins. J Neuroimmunol. 1990; 30:81–93. [PubMed: 1977769]
19. Guvenc H, et al. Impairment of glioma stem cell survival and growth by a novel inhibitor for Survivin-Ran protein complex. Clin Cancer Res. 2013; 19:631–642. [PubMed: 23251006]
20. Tran CT, et al. Differential expression of MHC class II molecules by microglia and neoplastic astroglia: relevance for the escape of astrocytoma cells from immune surveillance. Neuropathol Appl Neurobiol. 1998; 24:293–301. [PubMed: 9775395]
21. Ludwig HC, et al. Expression of nitric oxide synthase isozymes (NOS I–III) by immunohistochemistry and DNA in situ hybridization. Correlation with macrophage presence, vascular endothelial growth factor (VEGF) and oedema volumetric data in 220 glioblastomas. Anticancer Res. 2000; 20:299–304. [PubMed: 10769671]
22. Mizutani M, et al. The fractalkine receptor but not CCR2 is present on microglia from embryonic development throughout adulthood. J Immunol. 2012; 188:29–36. [PubMed: 22079990]
23. Ginestier C, et al. ALDH1 is a marker of normal and malignant human mammary stem cells and a predictor of poor clinical outcome. Cell Stem Cell. 2007; 1:555–567. [PubMed: 18371393]
24. Singh SK, et al. Identification of human brain tumour initiating cells. Nature. 2004; 432:396–401. [PubMed: 15549107]
25. Barker N, et al. Crypt stem cells as the cells-of-origin of intestinal cancer. Nature. 2009; 457:608–611. [PubMed: 19092804]
26. Bao S, et al. Glioma stem cells promote radioresistance by preferential activation of the DNA damage response. Nature. 2006; 444:756–760. [PubMed: 17051156]
27. Cheng L, et al. Glioblastoma stem cells generate vascular pericytes to support vessel function and tumor growth. Cell. 2013; 153:139–152. [PubMed: 23540695]
28. Calabrese C, et al. A perivascular niche for brain tumor stem cells. Cancer Cell. 2007; 11:69–82. [PubMed: 17222791]
29. Du R, et al. HIF1alpha induces the recruitment of bone marrow-derived vascular modulatory cells to regulate tumor angiogenesis and invasion. Cancer Cell. 2008; 13:206–220. [PubMed: 18328425]
30. Li Z, et al. Hypoxia-inducible factors regulate tumorigenic capacity of glioma stem cells. Cancer Cell. 2009; 15:501–513. [PubMed: 19477429]
31. Lathia JD, Heddleston JM, Venere M, Rich JN. Deadly teamwork: neural cancer stem cells and the tumor microenvironment. Cell Stem Cell. 2011; 8:482–485. [PubMed: 21549324]
32. Yang I, Han SJ, Sughrue ME, Tihan T, Parsa AT. Immune cell infiltrate differences in pilocytic astrocytoma and glioblastoma: evidence of distinct immunological microenvironments that reflect tumor biology. J Neurosurg. 2011; 115:505–511. [PubMed: 21663411]
33. Xing F, et al. Hypoxia-induced Jagged2 promotes breast cancer metastasis and self-renewal of cancer stem-like cells. Oncogene. 2011; 30:4075–4086. [PubMed: 21499308]
34. Auffinger B, et al. Conversion of differentiated cancer cells into cancer stem-like cells in a glioblastoma model after primary chemotherapy. Cell Death Differ. 2014; 21:1119–1131. [PubMed: 24608791]
35. Deininger MH, Pater S, Strik H, Meyermann R. Macrophage/microglial cell subpopulations in glioblastoma multiforme relapses are differentially altered by radiochemotherapy. J Neurooncol. 2001; 55:141–147. [PubMed: 11859968]

36. Bao S, et al. Periostin potently promotes metastatic growth of colon cancer by augmenting cell survival via the Akt/PKB pathway. Cancer Cell. 2004; 5:329–339. [PubMed: 15093540]
37. Baril P, et al. Periostin promotes invasiveness and resistance of pancreatic cancer cells to hypoxia-induced cell death: role of the beta4 integrin and the PI3k pathway. Oncogene. 2007; 26:2082–2094. [PubMed: 17043657]
38. Malanchi I, et al. Interactions between cancer stem cells and their niche govern metastatic colonization. Nature. 2012; 481:85–89. [PubMed: 22158103]
39. Michaylira CZ, et al. Periostin, a cell adhesion molecule, facilitates invasion in the tumor microenvironment and annotates a novel tumor-invasive signature in esophageal cancer. Cancer Res. 2010; 70:5281–5292. [PubMed: 20516120]
40. Koronyo-Hamaoui M, et al. Attenuation of AD-like neuropathology by harnessing peripheral immune cells: local elevation of IL-10 and MMP-9. J Neurochem. 2009; 111:1409–1424. [PubMed: 19780903]
41. Jin X, Ishii H, Bai Z, Itokazu T, Yamashita T. Temporal changes in cell marker expression and cellular infiltration in a controlled cortical impact model in adult male C57BL/6 mice. PLoS One. 2012; 7:e41892. [PubMed: 22911864]
42. Saederup N, et al. Selective chemokine receptor usage by central nervous system myeloid cells in CCR2-red fluorescent protein knock-in mice. PLoS One. 2010; 5:e13693. [PubMed: 21060874]
43. Movahedi K, et al. Different tumor microenvironments contain functionally distinct subsets of macrophages derived from Ly6C(high) monocytes. Cancer Res. 2010; 70:5728–5739. [PubMed: 20570887]
44. Qian BZ, Pollard JW. Macrophage diversity enhances tumor progression and metastasis. Cell. 2010; 141:39–51. [PubMed: 20371344]
45. Sica A, Mantovani A. Macrophage plasticity and polarization: in vivo veritas. J Clin Invest. 2012; 122:787–795. [PubMed: 22378047]
46. Yu JL, Rak JW. Host microenvironment in breast cancer development: inflammatory and immune cells in tumour angiogenesis and arteriogenesis. Breast Cancer Res. 2003; 5:83–88. [PubMed: 12631386]
47. Condeelis J, Pollard JW. Macrophages: obligate partners for tumor cell migration, invasion, and metastasis. Cell. 2006; 124:263–266. [PubMed: 16439202]
48. Sica A, Schioppa T, Mantovani A, Allavena P. Tumour-associated macrophages are a distinct M2 polarised population promoting tumour progression: potential targets of anti-cancer therapy. Eur J Cancer. 2006; 42:717–727. [PubMed: 16520032]
49. Sharda DR, et al. Regulation of macrophage arginase expression and tumor growth by the Ron receptor tyrosine kinase. J Immunol. 2011; 187:2181–2192. [PubMed: 21810604]
50. Arranz A, et al. Akt1 and Akt2 protein kinases differentially contribute to macrophage polarization. Proc Natl Acad Sci U S A. 2012; 109:9517–9522. [PubMed: 22647600]
51. Rolny C, et al. HRG inhibits tumor growth and metastasis by inducing macrophage polarization and vessel normalization through downregulation of PlGF. Cancer Cell. 2011; 19:31–44. [PubMed: 21215706]
52. Wang H, et al. Activated macrophages are essential in a murine model for T cell-mediated chronic psoriasiform skin inflammation. J Clin Invest. 2006; 116:2105–2114. [PubMed: 16886059]
53. Gillan L, et al. Periostin secreted by epithelial ovarian carcinoma is a ligand for alpha(V)beta(3) and alpha(V)beta(5) integrins and promotes cell motility. Cancer Res. 2002; 62:5358–5364. [PubMed: 12235007]
54. Butcher JT, Norris RA, Hoffman S, Mjaatvedt CH, Markwald RR. Periostin promotes atrioventricular mesenchyme matrix invasion and remodeling mediated by integrin signaling through Rho/PI 3-kinase. Dev Biol. 2007; 302:256–266. [PubMed: 17070513]
55. Grkovich A, Johnson CA, Buczynski MW, Dennis EA. Lipopolysaccharide-induced cyclooxygenase-2 expression in human U937 macrophages is phosphatidic acid phosphohydrolase-1-dependent. J Biol Chem. 2006; 281:32978–32987. [PubMed: 16950767]
56. Shrivastav A, et al. Requirement of N-myristoyltransferase 1 in the development of monocytic lineage. J Immunol. 2008; 180:1019–1028. [PubMed: 18178842]

57. Stupp R, et al. Phase I/IIa study of cilengitide and temozolomide with concomitant radiotherapy followed by cilengitide and temozolomide maintenance therapy in patients with newly diagnosed glioblastoma. J Clin Oncol. 2010; 28:2712–2718. [PubMed: 20439646]
58. Mantovani A, Sozzani S, Locati M, Allavena P, Sica A. Macrophage polarization: tumor-associated macrophages as a paradigm for polarized M2 mononuclear phagocytes. Trends Immunol. 2002; 23:549–555. [PubMed: 12401408]
59. Kim DW, et al. High tumour islet macrophage infiltration correlates with improved patient survival but not with EGFR mutations, gene copy number or protein expression in resected non-small cell lung cancer. Br J Cancer. 2008; 98:1118–1124. [PubMed: 18283317]
60. Popivanova BK, et al. Blockade of a chemokine, CCL2, reduces chronic colitis-associated carcinogenesis in mice. Cancer Res. 2009; 69:7884–7892. [PubMed: 19773434]
61. Qian BZ, et al. CCL2 recruits inflammatory monocytes to facilitate breast-tumour metastasis. Nature. 2011; 475:222–225. [PubMed: 21654748]
62. Pyonteck SM, et al. Deficiency of the macrophage growth factor CSF-1 disrupts pancreatic neuroendocrine tumor development. Oncogene. 2012; 31:1459–1467. [PubMed: 21822305]
63. Spear P, Barber A, Rynda-Apple A, Sentman CL. Chimeric antigen receptor T cells shape myeloid cell function within the tumor microenvironment through IFN-gamma and GM-CSF. J Immunol. 2012; 188:6389–6398. [PubMed: 22586039]
64. Germano G, et al. Role of macrophage targeting in the antitumor activity of trabectedin. Cancer Cell. 2013; 23:249–262. [PubMed: 23410977]
65. Guryanova OA, et al. Nonreceptor tyrosine kinase BMX maintains self-renewal and tumorigenic potential of glioblastoma stem cells by activating STAT3. Cancer Cell. 2011; 19:498–511. [PubMed: 21481791]
66. Huang Z, et al. Deubiquitylase HAUSP stabilizes REST and promotes maintenance of neural progenitor cells. Nat Cell Biol. 2011; 13:142–152. [PubMed: 21258371]
67. Cheng L, et al. Glioblastoma stem cells generate vascular pericytes to support vessel function and tumor growth. Cell. 2013; 153:139–152. [PubMed: 23540695]
68. Fang X, et al. The zinc finger transcription factor ZFX is required for maintaining the tumorigenic potential of glioblastoma stem cells. Stem Cells. 2014; 32:2033–2047. [PubMed: 24831540]

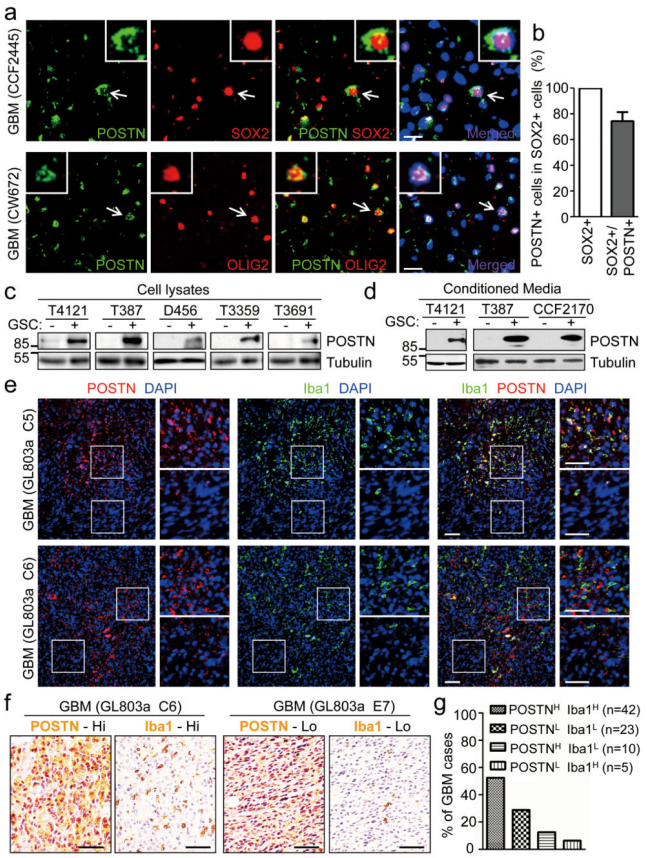

Figure 1. POSTN is preferentially secreted by GSCs and its levels correlate with TAM density in GBMs

a, Immunofluorescent staining of POSTN (green) and the GSC marker OLIG2 or SOX2 (red) in human primary GBMs. Frozen sections of GBMs (CCF2445 and CW672) were immunostained with antibodies against POSTN and SOX2 or OLIG2, and counterstained with DAPI to show nuclei (blue). POSTN was preferentially expressed in GSCs and distributed in the area near GSCs. Scale bar, 20μm. **b**, Graphical analysis of (**a**) showing the fraction of POSTN+ cells in SOX2+ cells (GSCs) in human primary GBMs. More than 70% of SOX2 positive GSCs showed POSTN staining (n=5 GBMs; mean ± s.e.m.). **c** and **d**, Immunoblot analysis of POSTN expression in cell lysates (**c**) and conditioned media (CM) (**d**) from GSCs (+) and matched non-stem tumor cells (−). CMs were obtained by culturing equal numbers of GSCs and non-stem tumor cells in Neurobasal media without supplements for 24 hours and concentrating media by vacuum centrifugation. Endogenous tubulin amounts in the corresponding cells were used for control. **e,** Immunofluorescent analysis of POSTN (red) and the TAM marker Iba1 (green) in GBM tissue microarray (US Biomax). Two sets of representative staining were presented to show the enrichment of TAMs in POSTN abundant regions in GBMs. Areas indicated with squares were enlarged and shown on right side of each picture. Scale bar, 80μm. **f,** Immunohistochemical staining of POSTN and the TAM marker Iba1 in two consecutive tissue microarray slides, respectively. Representative staining images show that the GBM (GL803a-C6) with higher POSTN levels contained more Iba1+ cells (TAMs) and the GBM (GL803a-E7) with lower POSTN levels

has less Iba1+ (TAMs). Scale bar, 40μm. **g**, Graphical analysis of POSTN and Iba1 staining in the tissue microarray slides. 52.5% of GBM cases showed $POSTN^{High}$ and $Iba1^{High}$ staining, and 28.75% of GBM cases showed $POSTN^{Low}$ and $Iba1^{Low}$ staining. Only 12.5% of GBM cases showed $POSTN^{High}$ but $Iba1^{Low}$ staining, and 6.25% of GBM cases showed $POSTN^{Low}$ but $Iba1^{High}$ staining. The majority (81.25%) of GBM cases showed that POSTN levels positively correlate with TAM density. (Data from 80 tumors).

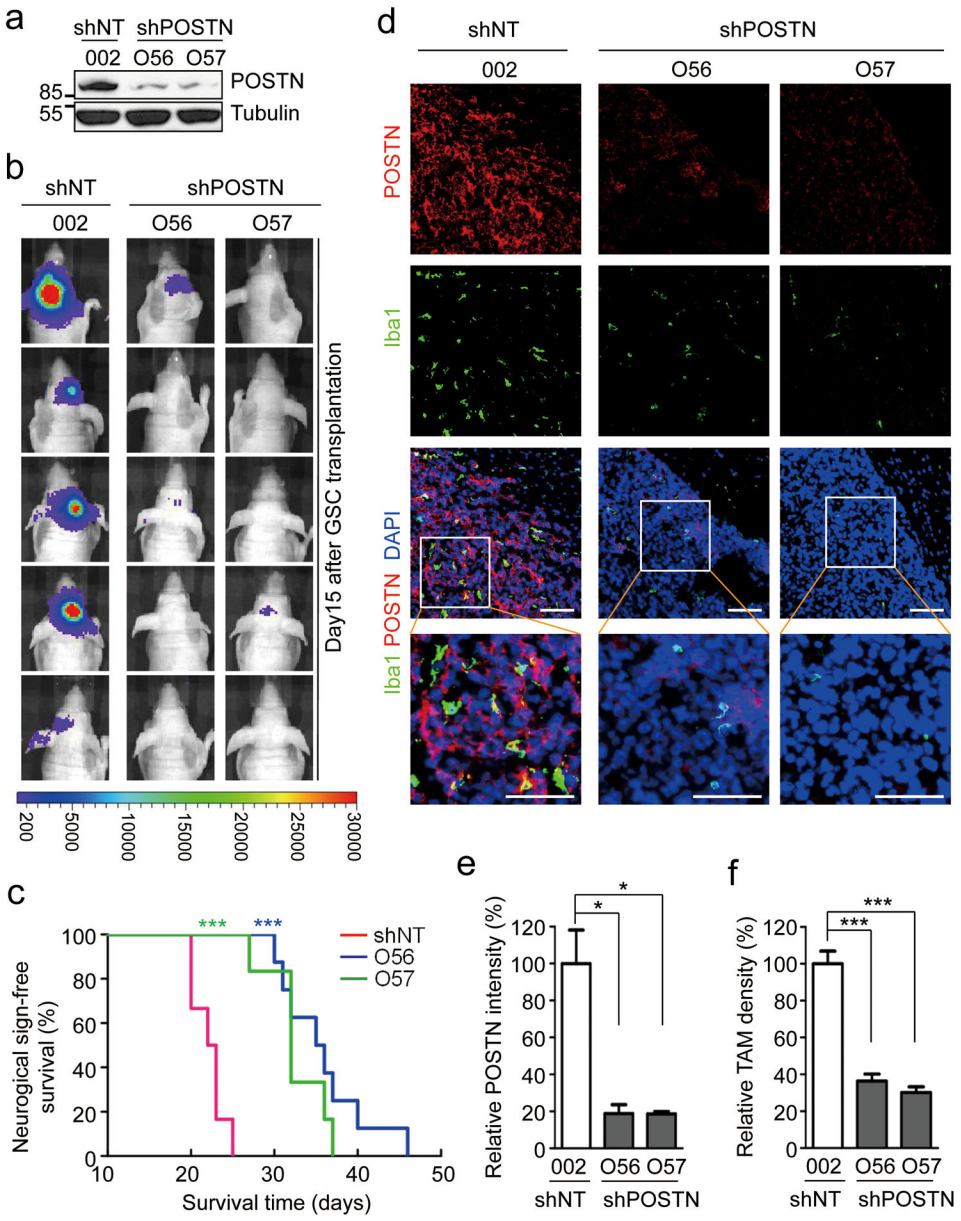

Figure 2. Disrupting POSTN by shRNA markedly inhibited tumor growth and reduced TAM density in GSC-derived xenografts

a, Immunoblot analysis of POSTN in GSCs expressing non-targeting shRNA (shNT) or POSTN shRNA (shPOSTN). Targeting POSTN by two distinct shRNA clones O56 and O57 through lentiviral infection reduced POSTN expression by 85–90% in GSCs (T387). **b,** *In vivo* bioluminescent imaging analysis of tumor growth in mice bearing GBM xenografts derived from GSCs expressing shNT or shPOSTN. GSCs (T387) were transduced with firefly luciferase and shPOSTN or shNT and then engrafted intracranially into athymic nude mice. Representative images on day 15 post transplantation were shown (data from 5 mice). Silencing POSTN by both O56 and O57 shRNA clones dramatically delayed tumor growth. **c**, Kaplan-Meier survival curves of mice implanted with GSCs expressing shPOSTN or

shNT (control). GSCs were transduced with shPOSTN (O56 or O57) or shNT through lentiviral infection and then were transplanted intracranially into athymic nude mice (20,000 cells per mouse). Survival curves were analyzed by two-tailed log-rank test. Mice bearing GSC-derived tumors expressing shPOSTN showed a significant survival extension relative to the control group. ***, $p<0.001$ (n=6 mice for shNT and O57, and n=8 mice for O56). **d,** Immunofluorescent analysis of POSTN (red) and the TAM marker Iba1 (green) in GBM tumors derived from GSCs expressing shPOSTN or shNT. Frozen sections of GBM tumors derived from GSCs with shPOSTN (O56 and O57) or shNT were immunostained with antibodies against POSTN and Iba1 and counterstained with DAPI (blue). Marked reductions of POSTN and Iba1 (TAMs) signals were detected in the GSC-derived tumors expressing shPOSTN. Scale bar, 80μm. **e** and **f**, Graphical analyses of (**d**) showing a decrease of POSTN signal intensity by ~80% and a significant reduction of TAM density by ~60% in the GSC-derived tumors expressing shPOSTN. POSTN intensity and TAM density were analyzed with ImageJ. *, $p<0.05$; ***, $p<0.001$ (n=5 tumors; mean ± s.e.m.; two tailed unpaired *t*-test).

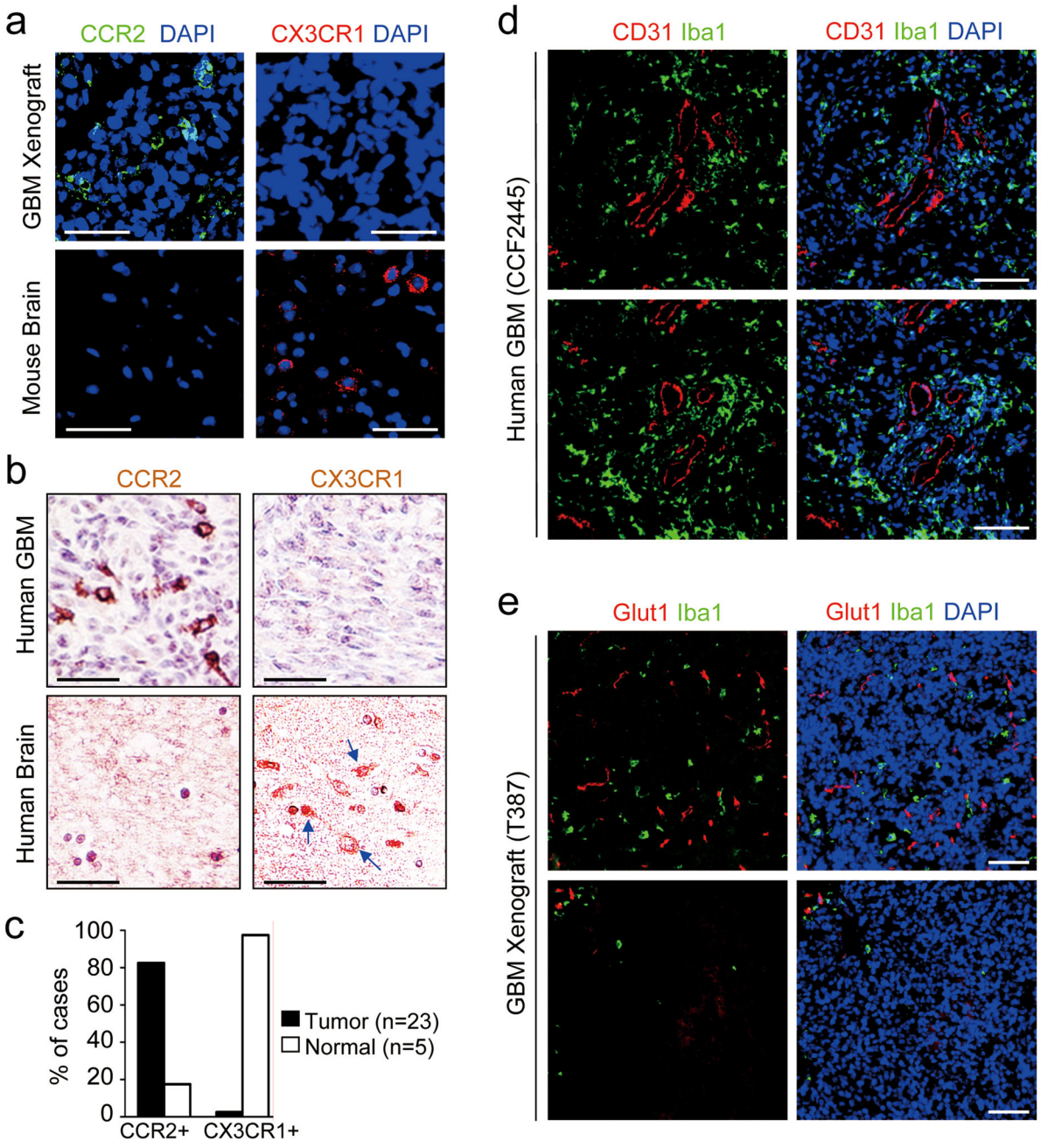

Figure 3. TAMs in human primary GBMs and xenografts are monocyte-derived macrophages from peripheral blood

a, Immunofluorescent staining of CCR2 (the marker for monocyte-derived macrophages) and CX3CR1 (the microglia marker) in GBM xenograft and normal brain tissue. Frozen sections of GSC-derived tumor (T387) and the adjacent normal mouse brain were immunostained with antibodies against CCR2 (green) and CX3CR1 (red) and counterstained with DAPI (blue). $CCR2^{+}$ cells were detected only in tumor tissue, while $CX3CR1^{+}$ cells were detected only in normal brain. Scale bar, 40μm. **b**, Immunohistochemical staining of CCR2 and CX3CR1 in human primary GBMs and normal brain tissue. Two consecutive

tissue microarray slides (US Biomax) containing GBMs and normal brain tissues were immunostained with antibody against CCR2 or CX3CR1 (brown) and counterstained with hematoxylin. GBM tumors showed abundant $CCR2^+$ cells (the monocyte-derived TAMs) but not $CX3CR1^+$ cells (microglia), while normal brain tissues contained $CX3CR1^+$ cells but not $CCR2^+$ cells. Scale bar, 40μm. **c**, Graphical analysis of (**b**) in tissue microarrays showed that $CCR2^+$ cells (monocyte-derived TAMs) were detected in the majority (82.6%) of GBM cases (data from 23 tumors) and the minority (20%) of normal brains (data from 5 normal samples). In contrast, $CX3CR1^+$ cells (microglia) were detected in all normal brains but only 4.3% of GBM tumor cases. **d**, Immunofluorescent staining of Iba1 and the CD31 in human primary GBMs. Frozen sections of a primary GBM (CW2445) were immunostained with antibodies against Iba1 to label TAMs (green) and CD31 to mark vessels (red) and counterstained with DAPI (blue). Abundant TAMs are enriched in perivascular niches. Scale bar, 80μm. **e**, Immunofluorescent staining of the TAM marker Iba1 and the endothelial marker Glut1 in GSC-derived xenografts. Frozen sections of GBM xenografts derived from GSCs (T387) were immunostained with antibodies against Iba1 (green) and Glut1 (red) and counterstained with DAPI (blue). TAMs (green) were localized near vessels but not in the area lacking blood vessel. Scale bar, 80μm.

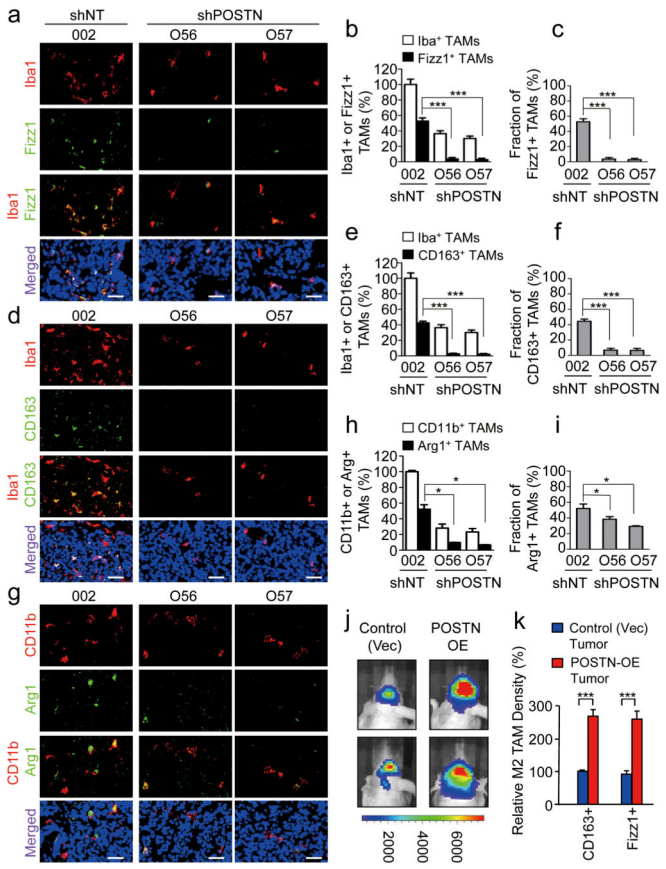

Figure 4. POSTN-recruited TAMs are maintained as M2 subtype in GSC-derived xenografts

a, Immunofluorescent staining of the M2 TAM marker Fizz1 (green) and the pan macrophage marker Iba1 (red) in GSC-derived tumors expressing shPOSTN (O56 and O57) or shNT (control). Nuclei were counterstained with DAPI (blue)). Scale bar, 40μm. **b** and **c**, Graphical analyses of (**a**) showing a significant reduction of Fizz1^{+} M2 subtype TAM density (**b**) and ratio (**c**) in shPOSTN-expressing xenografts relative to shNT-expressing xenografts. Relative M2 TAM density was normalized to total TAMs in shNT expressing xenografts. The M2 TAM fraction (ratio) was determined by the percentage of M2 TAMs within TAM population in shNT or shPOSTN xenografts, respectively. ***, $p<0.001$ (n=5 tumors; mean ± s.e.m.; two tailed unpaired *t*-test). **d,** Immunofluorescent staining of the M2 TAM marker CD163 (green) and the pan macrophage marker Iba1 (red) in GSC-derived tumors expressing shPOSTN or shNT. Scale bar, 40μm. **e** and **f**, Graphical analyses of (**d**) showing a significant reduction of CD163^{+} M2 subtype TAM density (**e**) and ratio (**f**) in shPOSTN-expressing xenografts relative to shNT-expressing xenografts. ***, $p<0.001$ (n=5 tumors; mean ± s.e.m.; two tailed unpaired *t*-test). **g,** Immunofluorescent staining of the M2 TAM marker Arg1 (green) and the pan macrophage marker CD11b (red) in GSC-derived tumors expressing shPOSTN or shNT. Scale bar, 40μm. **h** and **i**, Graphical analyses of (**g**) showing a significant reduction of Arg1^{+} M2 subtype TAM density (**h**) and ratio (**i**) in shPOSTN-expressing xenografts relative to shNT-expressing xenografts. *, $p<0.05$ (n=5 tumors; mean ± s.e.m.; two tailed unpaired *t*-test). **j,** *In vivo* bioluminescent imaging showing the accelerated tumor growth of intracranial xenografts from POSTN-

overexpressing (POSTN-OE). Representative images on day 16 post transplantation were shown (data from 5 mice). **k,** Graphical analysis of tumors in (**j**) showing an increase of M2 TAMs in xenografts overexpressing POSTN relative to the control tumor (vector). Frozen sections were stained with the M2 TAM marker CD163 or Fizz1 together with the vessel marker Glut1. $CD163^{+}$ and $Fizz1^{+}$ cell numbers were normalized to vessel density. ***, $p<0.001$ (n=5 tumors; mean ± s.e.m.; two tailed unpaired *t*-test).

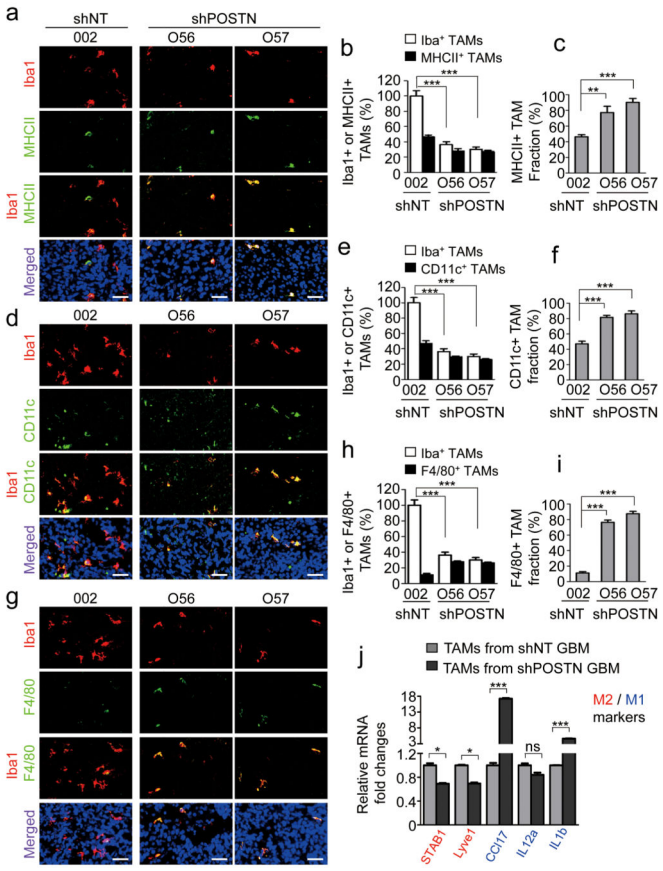

Figure 5. Silencing POSTN in GSCs increased relative fraction of M1 subtype TAMs in GSC-derived xenografts

a, Immunofluorescent staining of the M1 TAM marker MHCII (green) and the pan macrophage marker Iba1 (red) in GSC-derived tumors expressing shPOSTN or shNT (control). Nuclei were counterstained with DAPI (blue). Scale bar, 40μm. **b** and **c**, Graphical analyses of (**a**) showing the reduced TAM density (**b**) but the increased MHCII^{+} M1 fraction (**c**) in shPOSTN-expressing tumors relative to shNT expressing tumors. Relative TAM density was normalized to total TAMs in shNT expressing xenografts. The M1 TAM fraction was determined by the percentage of M1 TAMs within TAMs in shNT or shPOSTN xenografts, respectively. ***, $p<0.001$; **, $p<0.01$ (n=5 tumors; mean ± s.e.m.; two tailed unpaired *t*-test). **d,** Immunofluorescent staining of the M1 TAM marker CD11c (green) and the pan macrophage marker Iba1 (red) in GSC-derived tumors expressing shPOSTN or shNT. Scale bar, 40μm. **e** and **f**, Graphical analyses of (**d**) showing the reduced TAM density (**e**) but the increased CD11c^{+} M1 fraction (**f**) in shPOSTN-expressing tumors relative to shNT expressing tumors. ***, $p<0.001$ (n=5 tumors; mean ± s.e.m.; two tailed unpaired *t*-test). **g,** Immunofluorescent staining of the mature TAM marker F4/80 (green) and the pan macrophage marker Iba1 (red) in GSC-derived tumors expressing shPOSTN or shNT. Scale bar, 40μm. **h** and **i**, Graphical analyses of (**g**) showing the reduced TAM density (**h**) but the increased F4/80^{+} mature TAM fraction (**i**) in shPOSTN-expressing tumors relative to shNT expressing tumors. ***, $p<0.001$ (n=5 tumors; mean ± s.e.m.; two tailed unpaired *t*-test). **j,** qPCR analysis of multiple M1 and M2 macrophage markers in CD11b^{+} populations from

shNT-expressing or shPOSTN-expressing xenografts. M2 macrophage markers STAB1 and Lyve1 were significantly down-regulated in $CD11b^+$ population isolated from shPOSTN-expressing xenografts, whereas M1 marker CCL17 and IL1b were markedly up-regulated. ***, $p<0.001$; *, $p<0.05$; ns, $p>0.05$ (mean ± s.e.m.; n = 3 biologically independent samples per group, one representative experiment shown, and the experiment was repeated 3 times).

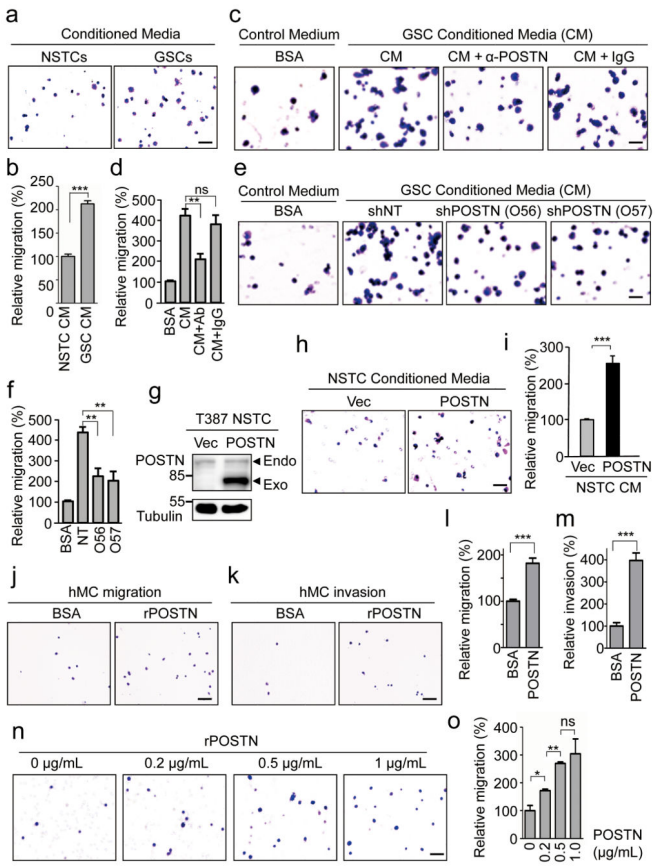

Figure 6. GSC-secreted POSTN is a chemoattractant to macrophages and monocytes

a, Representative images of migrated macrophage-like U937 cells toward conditioned media (CM) from matched T387 GSCs and non-stem tumor cells (NSTCs) in transwell assays. Scale bar, 80μm. **b**, Graphical analysis of (**a**) showing a significant increase of U937 cell migration toward GSC CM relative to NSTC CM. ***, $p<0.001$ (n=5 fields; mean ± s.e.m.; two-tailed unpaired *t*-test). **c**, Representative images of migrated U937 cells toward GSC CM pre-incubated with or without anti-POSTN (10μg/mL) antibody or IgG. Scale bar, 40μm. **d,** Graphical analysis of (**c**) showed that the increased macrophage migration toward GSC CM was attenuated by anti-POSTN antibody. **, $p<0.01$; ns, $p>0.05$. (n=5 fields; mean ± s.e.m.; two-tailed unpaired *t*-test). **e**, Representative images of migrated U937 cells toward CM from GSCs expressing shPOSTN (O56 and O57) or shNT. Scale bar, 40μm. **f**, Graphical analysis of (**e**) showing a significant reduction of migrated U937 cells toward CM from GSCs expressing shPOSTN. **, $p<0.01$ (n=5 fields; mean ± s.e.m.; two-tailed unpaired *t*-test). **g**, Immunoblot analysis of POSTN in NSTCs transduced with POSTN or vector control. **h**, Representative images of migrated U937 cells toward CM from POSTN-overexpressing or control NSTCs. Scale bar, 80μm. **i**, Graphical analysis of (**h**) showing a significant increase of U937 cell migration toward CM from POSTN-overexpressing NSTCs. ***, $p<0.001$ (n=5 fields; mean ± s.e.m.; two-tailed unpaired *t*-test). **j** and **k**, Representative images of cell migration (**j**) and invasion (**k**) of human primary monocytes toward recombinant POSTN (rPOSTN) in transwell assays. Scale bar, 80μm. **l** and **m**, Graphical analyses of (**j**) and (**k**) showing rPOSTN significantly promotes migration and

invasion of human monocytes/macrophages. ***, $p<0.001$ (n=5 fields; mean ± s.e.m.; two-tailed unpaired *t*-test). **n**, Representative images of migrated U937 cells toward different concentration of rPOSTN in transwell assays. Scale bar, 80μm. **o**, Graphical analysis of (**n**) showing that the migration of U937 macrophages toward rPOSTN protein was dose-dependent. *, $p<0.05$; **, $p<0.01$; ***, $p<0.001$; ns, $p>0.05$. (n=5 fields; mean ± s.e.m.; two-tailed unpaired *t*-test). All transwell assays were repeated three times.

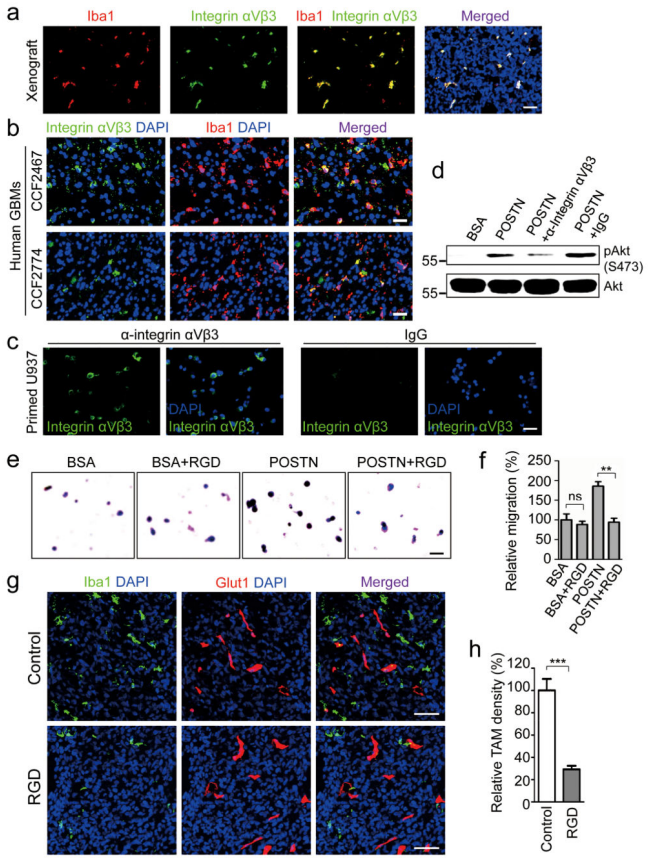

Figure 7. POSTN mediates through $\alpha_V\beta3$ integrin signaling to recruit macrophages

a, Immunofluorescent staining of integrin $\alpha_V\beta3$ (green) and the TAM marker Iba1 (red) in GSC-derived xenografts. Nuclei were counterstained with DAPI (blue). TAMs (Iba1+) showed positive for integrin $\alpha_V\beta3$ in the tumors. Scale bar, 40μm. **b**, Immunofluorescent staining of integrin $\alpha_V\beta3$ (green) and Iba1 (red) in human primary GBMs. A fraction of TAMs (Iba1+) showed positive for integrin $\alpha_V\beta3$ in GBM tumors (CCF2774 and CCF2467). Scale bar, 40μm. **c**, Immunofluorescent staining of integrin $\alpha_V\beta3$ (green) in PMA-primed U937 cells. U937 cells were stained positive with anti-integrin $\alpha_V\beta3$ antibody. Scale bar, 40μm. **d**, Immunoblot analysis of POSTN-induced Akt activation that was attenuated by the antibody against integrin $\alpha_V\beta3$ in PMA-primed U937 cells. After serum starvation overnight, cells were incubated with 0.1mg/ml anti-integrin $\alpha_V\beta3$ antibody or control IgG for 1 hour followed by stimulation with 0.5mg/ml recombinant POSTN (rPOSTN) for 1 hour. Pre-incubation with anti-integrin $\alpha_V\beta3$ antibody but not the control IgG dramatically inhibited POSTN-induced phosphorylation of Akt. **e**, Representative images of migrated U937 cells toward rPOSTN in the presence of inhibitory RGD peptide in transwell assays. PMA-primed U937 cells pre-incubated with or without RGD peptide (1 mg/ml) were used for assessing cell migration toward rPOSTN protein (0.2 μg/mL) or 0.1% BSA. Scale bar, 40μm. **f**, Graphical analysis of (**e**) showing that pre-incubation of U937 cells with the RGD inhibitory peptide significantly reduced U937 cell migration toward rPOSTN. **, $p<0.01$; ns, $p>0.05$. (n=5 fields; mean ± s.e.m.; the experiment was repeated 3 times and analyzed by two tailed unpaired *t*-test). **g,** Immunofluorescent analysis of the

TAM marker Iba1 (green) and the vessel marker Glut1 (red) in GBM xenografts treated with RGD inhibitory peptide or control peptide. Scale bar, 80μm. **h**, Graphical analysis of (**g**) showing a significant reduction of TAM density by ~70% in the GBM tumors treated with the RGD inhibitory peptide. ***, $p<0.001$ (n=5 tumors; mean ± s.e.m.; two tailed unpaired *t*-test).

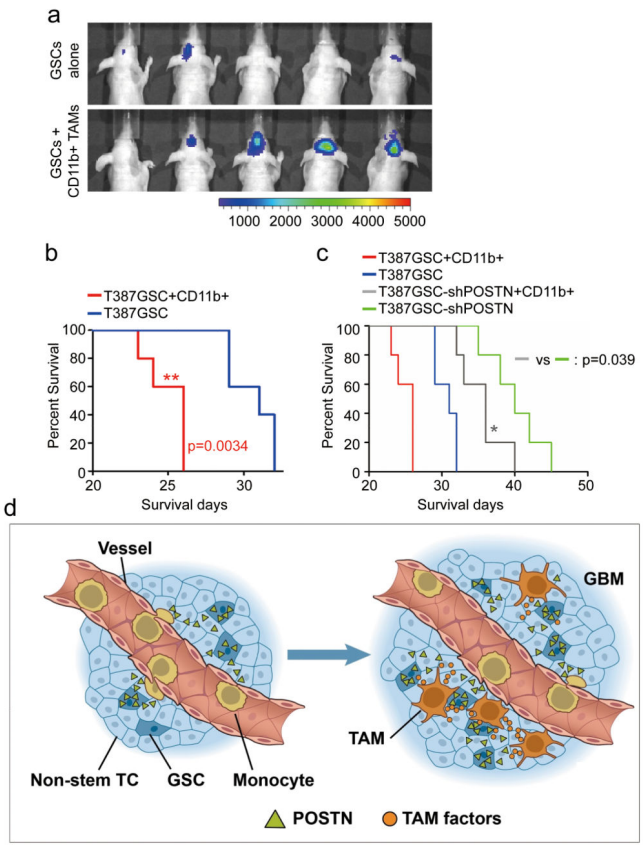

Figure 8. M2 subtype TAMs accelerated GSC tumor growth in mouse brains

a, *In vivo* bioluminescent imaging analysis of tumor growth in mice bearing GBM xenografts derived from GSCs plus CD11b$^+$ cells (enriched with M2 TAMs) or GSCs alone. 50, 000 CD11b$^+$ cells were isolated from GSC-derived xenografts and then co-transplanted with 20, 000 GSCs intracranially into athymic nude mice. Representative images on day 18 post transplantation were shown (data from 5 mice). Co-transplantation of GSCs with CD11b$^+$ TAMs dramatically promoted GSC tumor growth. **b**, Kaplan-Meier survival curves of mice implanted with GSCs plus CD11b$^+$ cells or GSCs alone. Mice implanted with T387 GSCs plus CD11b$^+$ cells showed a significantly shortened survival relative to the mice implanted with GSCs alone. p=0.0034. (n=5 mice for each group; two-tailed log-rank test). **c,** Kaplan-Meier survival curves of mice implanted with shPOSTN-expressing GSCs plus CD11b$^+$ cells or shPOSTN-expressing GSCs alone. Mice implanted with shPOSTN-expressing GSCs (GSC-shPOSTN) plus CD11b$^+$ cells showed a significantly reduced survival relative to the mice implanted with shPOSTN-expressing GSCs alone. p=0.039 (n=5 mice for each group; two-tailed log-rank test). **d**, A schematic representation of the POSTN-mediated recruitment of monocyte-derived TAMs from peripheral blood during GBM development. POSTN preferentially secreted by GSCs attracts monocytes from peripheral blood to enter GBM tissues. The POSTN-recruited, monocyte-derived TAMs are co-localized in perivascular niches with GSCs and maintained as M2 subtype macrophages that secret tumor supportive factors to promote GBM growth and progression.